Photo and particle induced transport of excited carriers in thin film tunnel junctions

D. A. Kovacs and J. Winter
Institut für Experimentalphysik II, Ruhr-Universität Bochum, D-44780 Bochum, Germany

S. Meyer and A. Wucher
Institut für Experimentalphysik, Universität Duisburg-Essen, D-47057 Duisburg, Germany

D. Diesing*
Institut für Physikalische Chemie, Universität Duisburg-Essen, D-45141 Essen, Germany
(Received 13 August 2007; published 6 December 2007)

Photo and particle induced charge carrier (electrons and holes) transport is studied in metal-insulator-metal tunnel junctions of Ag-AlO_x-Al type. The electronic excitation induced by photo irradiation with $h\nu = 4.67$ eV is compared with that induced by the impact of argon ions with a kinetic energy of 12 keV. The common feature of the two experiments is that only charge carriers with energies above (electrons) or below (holes) the tunnel barrier are detected. The electron to hole induced current ratio is adjustable by applying a bias voltage to the sample. A similar bias dependence of the induced current was found in both experiments. While the bias dependence of the photo induced current cannot be unambiguously explained due to the possibility of simultaneous excitation of both metal films, one can discuss the bias dependence of particle induced currents clearly in terms of electrons and holes excited in the top electrode only. Within a computer simulation based on a three dimensional model, we show that the photo induced conduction in Ag-AlO_x-Al junctions is mainly determined by the simultaneous excitation of electrons and holes in the top Ag film. Moreover, the model indicates that the dominant contribution to the induced current is given by the charge carriers excited near the silver-oxide interface. Finally, we show that the particle induced current can be modeled by carrier transport between two free-electron gases, excited to an elevated electron temperature and to room temperature, respectively. Hereby, the influence of the tunnel barrier parameters and the elevated electron temperature on the bias dependence is discussed.

DOI: 10.1103/PhysRevB.76.235408 PACS number(s): 73.40.Rw, 73.50.Pz

I. INTRODUCTION

Particle and photo induced electronic excitations at solid surfaces are an intensively studied field. Experiments investigating these processes are based on the detection of electrons with excess energy above the Fermi level. This can be reached by two different techniques: (i) When the excess energy is higher than the work function, electrons can be detected outside the sample by an electron spectrometer. (ii) With a lower excess energy, the detection succeeds by the transport over internal barriers which discriminates between ground state and excited electrons.[1]

The latter method has recently received new attention since the detection of chemically induced electronic excitations became possible with Schottky devices,[2] as well as with metal-insulator-metal (MIM) tunnel junctions.[3,4] In this type of experiments, excited carriers are detected which have enough energy to overcome either a Schottky or a tunnel barrier. Therefore, the metal film acts both as a substrate for the reaction and as an emitter of hot carriers. This special role points to one conceptional difficulty of this technique. The locations of electronic excitation (metal-vacuum interface) and detection (metal-semiconductor or metal-insulator interface) are separated by several nanometers of metal, meaning that a carrier distribution resulting from the convolution of an excitation spectrum and a transport process is detected.

The variation of the metal electrode thickness is one possibility to understand the influence of excited carrier transport on the detected signals.[5,6] The transport of excited electrons through a thin metal film and the subsequent crossing of a metal-semiconductor interface has already been intensively investigated in photo excitation experiments. On the basis of work on photo emission from semiconductors[7,8] and the use of Schottky and tunnel devices for the detection of weakly excited electrons,[1] Kane described the detection of transported photo excited electrons in Schottky diodes.[9] His work was extended by a random walk model including energy dependent mean free paths,[10] which were applied later to MIM structures.[11] The calculation of photo induced currents in such systems is even more difficult since both metal electrodes may work as photo emitters. Another complication results from the fact that besides electrons, also holes are excited, which can, in principle, also tunnel and contribute to the measured current. MIM devices offer, however, the possibility to discriminate between the contribution of electrons and holes to the induced tunneling current by applying a bias voltage between the two metal electrodes.

In Fig. 1(a), a schematic drawing of a MIM device is presented. In our work, it consists of a bottom metal film (aluminum) with a thickness of about 50 nm and a top metal film (silver) with the thickness in the range of 10–100 nm, separated by a very thin insulator layer (aluminum oxide) with a thickness of 4 nm. As shown in Sec. IV, the tunneling probability through the oxide for an excited carrier of excess energy E is related to the energy deficit of the carrier. In a two-band model, this is defined as the minimum excess energy needed by the carrier to surmount the potential barrier

 ©2007 The American Physical Society

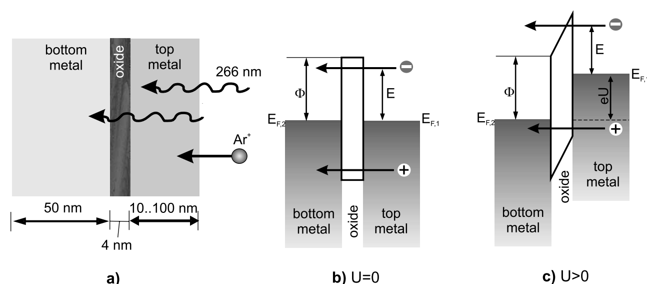

FIG. 1. (a) Schematic drawing and (b) energy diagram of metal-insulator-metal (MIM) sandwich structure at $U=0$ V (continuous lines) and at $U>0$ V (dashed lines).

via the conduction band for electrons or via the valence band of the oxide for defect electrons ("holes"), respectively, as illustrated in Fig. 1(b). The tunneling probability of the carriers can be modified by applying a bias voltage between the two metals. Thus, when the bottom electrode is at a more positive potential than the top (exposed) electrode, the Fermi level E_F of the latter is shifted to higher energies by an amount eU, where U is the bias voltage, which we define to be positive in this case. As a consequence, the potential barrier is sheared as illustrated in Fig. 1(c). The result is that the energy deficit is lowered for the hot electrons and enhanced for the hot holes, since for the electrons the mean barrier height (the average value across the oxide layer) is reduced, while for the holes it is raised. For a negative bias voltage, the opposite effect occurs. In this way, it is possible to amplify the electron contribution and diminish the hole contribution to the measured current or vice versa. It should be mentioned that the shape of the tunnel barrier is given in Fig. 1(b) as rectangular only for simplicity and that a trapezoidal barrier does not change qualitatively the response of the barrier to the applied bias voltage.

An investigation of the photo induced conduction in Al-AlO_x-Al structures has been performed by Gundlach and Kadlec who varied the thickness of one metal electrode and thereby modified the ratio between the photo currents originating from absorption in the two metal films.[12] Their interpretation of the results was, however, ambiguous, since they could neither rule out the signal contribution of the thinner electrode nor quantify the influence of excited holes on the measured currents. A clear evidence for photo induced hole tunneling through thin alumina was shown by the experiments of Goodman, who used Al-AlO_x-H_2O junctions.[13] The employment of distilled de-ionized water as a counterelectrode was done to ensure that carriers are excited only in the Al electrode, water being known to be transparent in the investigated energy region 2–6 eV. Thus, by varying the photon energy, it was found that the photo induced current changes sign at 3.7 eV. Since no absorption and, hence, no carrier excitation were expected to occur in water, the current measured at energies higher than 3.7 eV was assigned to a net hole current flowing from Al into the aluminum oxide layer. Especially for amorphous aluminum oxide, the role of hole tunneling should not be underestimated since the band gap is reduced with respect to the band gap of, for instance, the crystalline sapphire.[14]

To avoid the mentioned ambiguity, we performed, for comparison, experiments dealing with particle induced electronic excitations (i.e., argon ions with variable kinetic energy) in the top electrode of a MIM structure. Due to the relatively low penetration depth of the projectiles, the particle induced excitation clearly resides in the top electrode of the sample only. Thus, a backward current (i.e., electron current flowing from the bottom to the top electrode) can be excluded.

In the present work, experimental as well as computer simulation results on photon and particle impact induced conduction in Ag-AlO_x-Al junctions are presented. The photo-induced conduction is investigated at $h\nu=4.67$ eV, whereas argon ions with a kinetic energy of 12 keV are employed as particles bombarding a silver surface. The photon energy was carefully chosen in order to fulfill two requirements: (i) $h\nu<6$ eV (band gap of the amorphous oxide) for avoidance of direct carrier excitation in the insulator and (ii) $h\nu>3$ eV (mean barrier height) for working with a signal-to-noise ratio of better than 10^3 without damaging the sample.

In both kinds of experiments, a bias voltage is applied to vary the electron to hole tunneling current ratio, this allowing to switch over from a hot electron to a hot hole dominated tunneling current. In addition, the thickness of the top silver film was varied in order to investigate the effect of hot carrier transport. The dependence of the photo induced current on both the bias voltage and silver film thickness is compared with results of a computer simulation based on the optical treatment of Kadlec,[11] the two-band tunneling model of Franz[15] and Kane and Blount,[16] and a quasithermal free-electron gas at elevated electron temperature representing the ion bombarded surface.

The present paper is organized as follows. In Sec. II, a brief description of the experimental setup is given. Section III is divided into two parts: one (Sec. III A) presenting results and discussions on photo induced conduction, and the second one (Sec. III B) dealing with the particle induced conduction in Ag-AlO_x-Al sandwich structures. In an attempt to explain the experimental data, computer simulations of the bias dependence are presented in Sec. IV. In particular, a photo conduction model for a two-band tunnel system is presented in Sec. IV A together with calculations obtained within this model. In order to simulate the kinetically induced tunneling current, a model describing the charge transport in a two-band tunnel system between free-electron gases at different temperatures is introduced in Sec. IV B, including results and discussions of the calculations performed within this model.

II. EXPERIMENT

The experiments with Ar^+ ions were carried out in an ultrahigh vacuum chamber with a base pressure of about 10^{-9} mbar. The primary ions were generated by a commercial ion gun delivering a focused and pulsed inert gas ion beam with energies between 5 and 15 keV and a current of a few hundred nanoamperes impinging under 45° with respect to the surface normal.[6]

The laser beam was produced in a pulsed Nd:YAG (yttrium aluminum garnet) laser system working at 1064 nm. In

the present work, the fourth harmonic (266 nm) having a maximum pulse energy of 5 mJ, a pulse width of 5 ns, and a repetition rate of 10 Hz was used. The energy per pulse was, however, reduced in our work to values below 0.1 mJ to avoid sample damaging.

The particle as well as the photo induced current flowing through the oxide barrier was measured with a three-step current-to-voltage converter connected to the Al electrode. MIM tunnel junctions as presented schematically in Fig. 1(a) have been used as samples in both experiments. They consist of a 50 nm thick aluminum film (bottom metal), an amorphous aluminum oxide layer with a thickness of 4 nm, and a silver film (top metal) with a thickness varying between 20 and 70 nm. The electrical quality of the samples was checked by measuring the dc tunneling current when applying a voltage ramp from −0.5 to 0.5 V with a scan rate of 50 mV/s. Besides a constant charging current, induced by the capacitance of the sample, the junction showed no measurable dc tunneling current in this range. For larger bias voltages, however, a dc tunneling current was registered even without excitation. Since we are only interested in the response of the system to external excitation by photon or particle impact, this dc current was subtracted from the measured data. For that purpose, the Ar^+ ion beam was operated in a pulsed mode with a pulse width of 10 ms and a repetition rate of 5 Hz, and the pulse response of the system was directly measured by time resolved registration of the tunneling current. During photo excitation, this was not possible due to the short pulse length (<10 ns) of the excitation laser. In this case, the laser was periodically switched off and on with a period of 20 s, and the signal recorded with the laser off was subtracted. The investigated bias voltage range was chosen such that the dc tunneling current did not exceed a value of 2-3 nA, since above 5 nA, the MIM was found to irreversibly change its properties. The detection limit for both particle and photo induced currents is restricted by a noise level of ±2 pA.

Since both the photo and particle induced tunneling currents are proportional to the intensity of the incoming photons and particles, respectively, we introduced the so-called internal emission yield γ to characterize the efficiency of the corresponding excitation process. The *photo induced* internal emission yield is defined as the net number of negative elementary charges flowing from the top to the bottom metal film through the oxide layer of the MIM junction per incident photon. It is determined as follows: (i) the tunneling current is integrated over a time period of 20 s when the laser is on, (ii) the number of laser pulses within the same 20 s is counted with the laser switched off, (iii) the number of photons in a laser pulse is determined as the measured pulse energy divided by photon energy, and (iv) from (ii) and (iii), the total number of photons incident in the time slot of 20 s is calculated. Finally, γ is given by the ratio of the integrated tunneling charge to the total number of incoming photons. The *particle induced* internal emission yield is defined as the net number of negative elementary charges flowing from the top to the bottom metal film through the oxide layer of the MIM junction per incident Ar^+ ion. It is determined by dividing the total tunneling charge by the total number of projectile ions. The former quantity is obtained by integrating the measured tunneling current over the pulse duration of 10 ms, while the latter is obtained by integrating the measured primary ion current over the same pulse. A negative yield denotes, in both definitions given above, a net number of negative elementary charges flowing from the bottom to the top metal electrode.

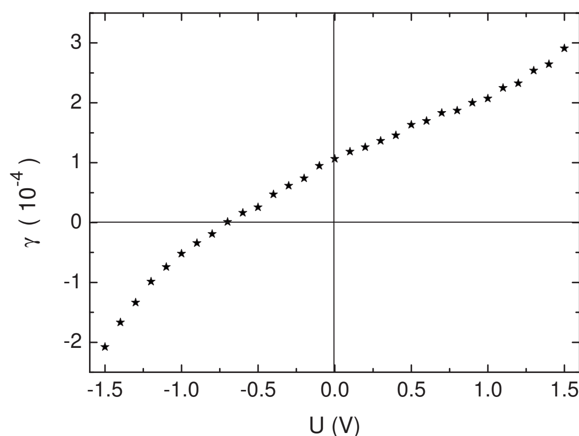

FIG. 2. Measured bias dependence of the photo induced internal emission yield at a photon energy ($h\nu$=4.67 eV) in a Ag-AlO_x-Al sandwich structure. The thickness of the silver film was 20 nm.

III. RESULTS AND DISCUSSION

A. Photo induced conduction

The dependence of the internal photo induced emission yield ($h\nu$=4.67 eV) on the applied bias voltage under normal incidence is plotted in Fig. 2. With applied voltage U=0 V, the yield per incident photon is about 1.1×10^{-4}. This relatively low value may be explained by the fact that most of the charge carriers are excited near the metal-vacuum interface and suffer inelastic collisions in the silver film losing, hence, a part of their energy. As a consequence, a part of the scattered carriers does not reach the metal-oxide interface, while the other part reaches it with less excess energy with respect to the Fermi level than they initially have. The (ballistic and scattered) carriers reaching the metal-oxide interface must then overcome the potential barrier of the oxide in order to contribute to the measured yield. Since the transmission probability through the barrier strongly decreases with decreasing energy and the transmission over the barrier ($E>\Phi$) is close to 1, the barrier acts practically as a "high-pass" filter. At positive bias voltages, the yield shows a practically linear increase up to about 1.0 V. At higher values, the yield departs slightly from this linear behavior, showing a stronger dependency on the voltage. At negative voltages, the yield decreases again linearly up to about −1.0 V, but with a different slope. At higher negative values, the yield-voltage dependence departs again from the linear behavior, again becoming steeper. The most interesting observation is, however, the sign reversal of the yield at −0.7 V, meaning that more electrons are flowing from the aluminum into the silver electrode than vice versa.

The attempt to explain the results presented above by taking into account only electrons flowing from the silver (top

electrode) into the aluminum layer (bottom electrode) fails, since with increasing negative voltage less and less electrons will find available states in the bottom electrode until no available free states will be found at all. From elementary quantum mechanical considerations, it can be shown that an exponentially decreasing yield would be expected when decreasing the voltage, if only electrons tunneling *through* the potential barrier, residing in states close to the silver Fermi level, were involved and if the tunneling were mediated only by the oxide conduction band (*one band model*). It will be shown below (see Sec. IV, Fig. 7), however, that even in such a one band model, a much weaker, almost linear behavior is found in the investigated voltage range. This indicates that the main contribution to the induced current is given by the high energy tail of the electron energy distribution at the metal-oxide interface in the region *above* the mean barrier height. Nevertheless, this behavior still cannot explain the observed sign change. Thus, it can be concluded that this sign change must be either due to reverse electron current flowing from the bottom into the top electrode or due to a hole current flowing from the top into the bottom electrode (or to a combination of both).

The first explanation was used by Shepard[17] for the sign reversal observed in a similar experiment. The possibility that a hole current can lead to such a polarity change was mostly ruled out[18] by assuming that the potential barrier for holes is much higher than that for electrons. In a one band model, this is natural because the energy deficit of states located below the Fermi level E_F must necessarily be larger than that of excited electrons in states above E_F. As mentioned above, a specific potential barrier for holes can only be introduced in a *two-band model*, i.e., assuming that the quantum mechanical transmission through the barrier is determined not solely by the presence of the conduction band but also by the presence of the valence band of the oxide. In this model, besides the thickness of the oxide, two parameters will determine the transmission: (i) the distance between the carrier energy level and the lower edge of the conduction band and (ii) the distance between the carrier energy level and the upper edge of the valence band. The latter, in turn, is determined by the band gap of the oxide [see Eq. (11)]. The resulting effective potential barrier heights for electrons and holes were usually estimated from the bulk properties of sapphire, i.e., a band gap of 8.3 eV, thus rendering the effective barrier for holes too large to permit a sizable hole contribution to the tunneling current. In the MIM sandwich structures produced here, however, the oxide film is amorphous, with its properties depending strongly on the preparation conditions. It has been shown that for thin chemically prepared films, the band gap can be as low as 6 eV,[19] resulting in comparable barrier heights for electrons and holes.

As illustrated in Fig. 3, the existence of a hole current can, at least qualitatively, account for the observed dependence of the yield on the voltage. At $U=0$ V, the main transport channels are illustrated in Fig. 3(a). Hot carriers may traverse the oxide layer either by quantum mechanical tunneling at low excitation energies (both electrons and holes) or by over-the-barrier propagation through the conduction band (electrons) or through the valence band (holes) at high excitation states.

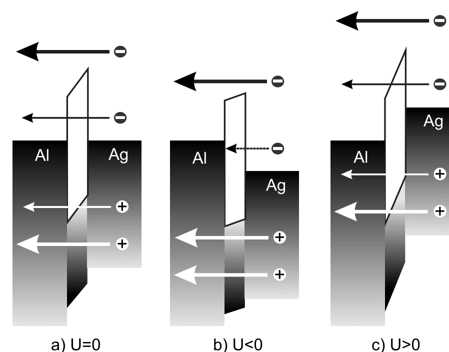

FIG. 3. Different channels in photo induced charge transfer and corresponding bias dependences. Thick (thin) arrows mean high (low) transmission probability. Trapezoidal shape at $U=0$ V due to the barrier asymmetry of 1.5 eV (Ref. 20).

With decreasing bias voltage ($U<0$ V) the transmission probability for the electrons through the oxide decreases due to two reasons: First, electrons with excess energies $E<eU$ are not able to tunnel anymore, since they cannot find available unoccupied states in the opposite metal. Second, the mean barrier height for electrons increases, since the barrier shape becomes more rectangular. In contrast, a lowering of the mean barrier height for holes will occur in this case, leading to an increase of the transmission probability. Therefore, the (decreasing) electron current will partly be counterbalanced by a (increasing) hole current, thus reducing the observed tunneling current. At a certain negative value of U, the hole current may even exceed the electron current, thus leading to the observed polarity change. With increasing bias voltage ($U>0$ V), the above argumentation applies again by interchanging electrons with holes. As a result, the net induced current flowing through the oxide layer increases.

We measured the photo induced tunneling current also by using the third harmonic of the laser ($E_{ph}=3.5$ eV). Although the photon energy was, in this case, by about 1.2 eV smaller, a sign reversal was observed around −0.7 V, too. Thus, the sign reversal appears not to depend on the photon energy and, hence, on the amount of energy dissipated in the electronic system. The lower value of the photon energy led, however, to a value $\gamma(0)$ which was by about 1 order of magnitude smaller than that measured for $E_{ph}=4.67$ eV. As checked by the two-temperature model presented in Sec. IV B 1, the crossover point rather describes the asymmetry, relative to the Fermi level, of the carrier energy distribution which passes the potential barrier, this being mainly determined by the asymmetry of the barrier relative to the Fermi level.

Figure 4 shows the measured normalized photo induced internal emission yield plotted against bias voltage for silver film thicknesses of 20, 30, and 40 nm, respectively. It can be noticed that all three curves change sign at the same value of the bias voltage. Moreover, it can be shown that the normalized function $\gamma(U)/\gamma(0)$ does not depend on the silver film thickness. In principle, this is a surprising result, since by increasing the silver film thickness, the total photo absorption in silver increases while in aluminum it decreases. Consequently, the relative contribution of the forward (from Ag

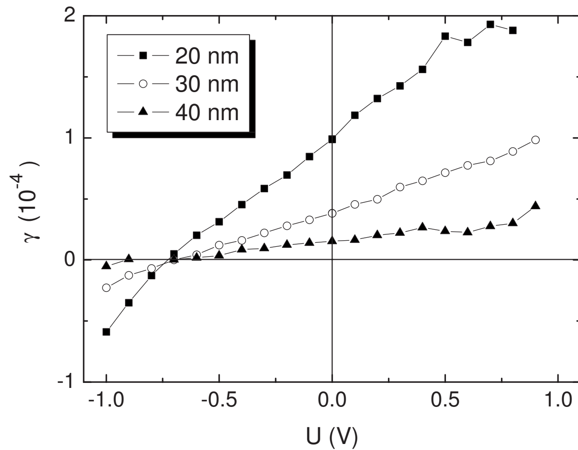

FIG. 4. Measured bias dependence of the photo induced current at a photon energy $h\nu$=4.67 eV in a Ag-AlO$_x$-Al junction, plotted for different values of the silver film thickness.

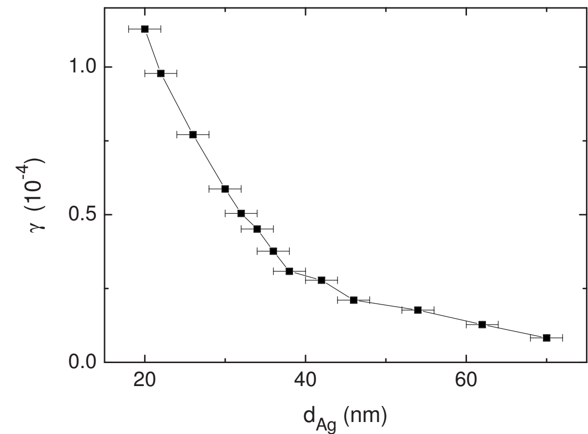

FIG. 5. Measured photo-induced internal emission yield at U =0 V in a Ag-AlO$_x$-Al junction, plotted against the thickness of the silver film.

into Al) and backward (from Al into Ag) currents to the net current and, hence, the bias dependence of the yield are expected to change. There are, however, two possible scenarios which may explain the experimental data in Fig. 4: (i) The relative contribution of the backward current to the measured yield is negligibly small. (ii) The yield is determined mainly by the carriers excited close to both metal-oxide interfaces.

The first scenario may occur when the number of absorbed photons in Al is negligibly small or/and if an electric field, repelling the carriers excited in Al, is present in the oxide. Assuming that this scenario sets in, the increasing silver film thickness leads to a shift of the depth distribution of excited electron-hole pairs toward the silver surface due to the attenuation of the light beam. This means that the mean propagation distance of the carriers to the metal-oxide interface increases. The resulting decrease of the net yield is then mainly influenced by the *carrier propagation* in the metal. At the same time, the normalized electron-hole energy distribution and, hence, the relative contribution of excited electrons and holes to the measured yield remain unchanged.

The second scenario implies energy loss during carrier transport in the metal and may occur if the mean free path of the excited charge carriers in the metal is much smaller than the film thickness. In this scenario, the number of excited carriers at the two metal-oxide interfaces decreases with film thickness, while the additionally created electron-hole pairs in the added silver layers are too far away from the metal-oxide interface and, thus, do not contribute to the measured yield. The resulting decrease of the net yield is then mainly given by the *light beam attenuation* in the metal. On the other hand, the relative contribution of forward and backward currents to the measured yield remains the same, since the normalized electron-hole energy distribution at both interfaces does not change.

To determine whether energy loss during carrier propagation or light beam attenuation is the dominant factor responsible for the decay of the yield with increasing silver film thickness, we also measured the thickness dependence of the photo induced internal emission yield in the range from 20 to 70 nm, at a bias voltage of 0 V, as plotted in Fig. 5. An exponential-like decay of the yield with increasing thickness can be observed. Thereby, the yield decreases from 1.1×10^{-4} at 20 nm to 8.3×10^{-6} at 70 nm silver. This corresponds to an exponentially decay factor of about 14 nm, which could be attributed, in principle, to both beam attenuation and carrier propagation. A more quantitative analysis based on computer simulation data will be presented in Sec. IV A 4.

B. Particle induced conduction

Figure 6 shows the bias dependence of the internal emission yield induced by an argon ion beam with a kinetic energy of 12 keV impinging onto a Ag-AlO$_x$-Al tunnel junction under an angle of incidence of 45°. A striking qualitative resemblance with the bias dependence of the photo induced current (see Fig. 2) can be noticed. Again, the experimental data can be fitted by two linear curves for voltages ranging from 0.7 to 0 V and from 0 to −0.7 V, respectively, departing slightly from this behavior at higher negative voltages.

Quantitatively, two aspects should be noticed. First, the particle induced emission yield takes values in the region of

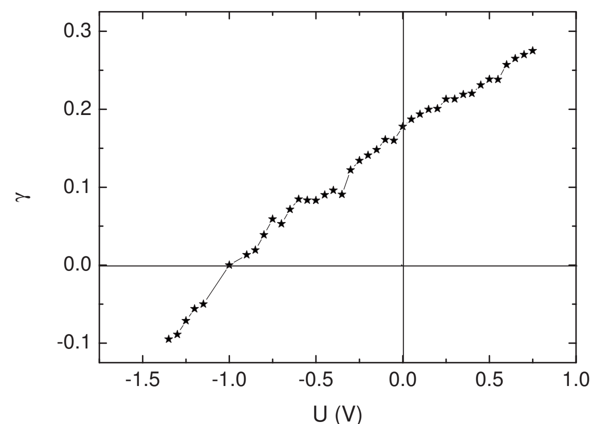

FIG. 6. Bias dependence of argon ion induced tunneling current in a Ag-AlO$_x$-Al sandwich structure. The kinetic energy of the Ar ions was 12 keV. Curve taken from Ref. 24.

0.1–1, being 3 orders of magnitude larger than the values obtained from the photo emission. These relatively large yields may be explained by the high energies involved, which lead to large amounts of dissipated energy and, hence, to more excited charge carriers in the silver film. The relatively large internal emission yields compare well with those measured for kinetic external electron emission generated by energetic ion impact under the prevailing bombarding conditions.[21]

A second observation is that the polarity change occurs here at about -1.0 V. Thus, compared to the photo induced emission, there is a shift of the cross over point by 0.3 V to higher negative values. It is clear that two different energy distributions of hot charge carriers cause the measured yield in the two kinds of experiments. Due to the high energies dissipated in the experiment with argon ions, not only more but also hotter electrons and holes are expected to be generated in the silver film, since particle impact with these kinetic energies also causes electron emission into the vacuum.[22]

Nevertheless, while the inelastic mean free path for electrons decreases with increasing energy up to about 20 eV,[23] holes excited below the bottom of the metal conduction band are practically immobile and can decay only in Auger processes producing further electron-hole pairs. As a result, the center of gravity of the transported hot electron-hole energy distribution is expected to shift to higher energies with respect to the photo induced one, thus causing a sign change of the induced current at a more negative bias voltage.

IV. THEORETICAL CONSIDERATIONS

A. Photo conduction in two-band systems

In order to understand the experimental results on photo conduction across the tunnel junction, we developed a computer code that simulates the photo induced current in MIM tunnel junctions within a simple model based on the work of Kadlec.[11] The photo conduction can be viewed as a three-step process: photo excitation, transport toward the barrier, and transmission over and/or through the potential barrier of the induced hot charge carriers. This three-step model is presented in the following within a detailed derivation of the photoinduced current in the Ag-AlO_x-Al system.

1. Photo excitation

The probability P_{exc} of a photon with energy E_{ph} (perpendicular incidence) to excite an electron at the depth z below the surface to an energy E (measured from the Fermi level E_F) can be factorized as[11]

$$P_{\mathrm{exc}}(E,z) = P_0(E)\,\eta(z), \tag{1}$$

where $P_{\mathrm{exc}}(E,z)$ will be called in the following *excitation function*, $P_0(E)$ is the *normalized distribution function* for electrons excited to energy E, and $\eta(z)$ is defined as the ratio of the number of photons absorbed per unit volume at the position z to the number of photons incident per unit area of the surface, being called *volumetric absorptance*.[25] It should be mentioned that Eq. (1) is valid only by assuming that each absorbed photon excites one and only one electron-hole pair. This assumption seems plausible, since our photon energy is far from the silver plasmon resonance at 3.8 eV,[26] rendering collective excitation improbable.

For a given ground-state distribution function $f(E)$ and a density of one-electron levels per unit volume $g(E)$ in the metal, and assuming the dipole matrix elements associated with the excitation process to be independent of energy, one can write

$$P_0(E) = \begin{cases} \dfrac{f(E')g(E')}{\int_{-E_F}^{\infty} f(E')g(E')dE'} & \text{if} \quad E>0 \\ 0 & \text{otherwise}, \end{cases} \tag{2}$$

with $E' = E - E_{\mathrm{ph}}$ and

$$f(E') = (e^{E'/k_BT}+1)^{-1}, \tag{3}$$

$$g(E') = \frac{3n_e}{2E_F^{3/2}}(E'+E_F)^{1/2}, \tag{4}$$

where E_F and n_e are the Fermi energy (5.49 and 11.7 eV for Ag and Al, respectively[27]) and the electron number density of the metal under consideration, respectively.

For simplicity, we treat the electrons in the free-electron approximation at a temperature of 0 K. In this case, Eq. (2) becomes

$$P_0(E) = \begin{cases} \dfrac{3}{2E_F^{3/2}}(E+E_F-E_{\mathrm{ph}})^{1/2} & \text{if} \quad 0<E<E_{\mathrm{ph}}, \\ 0 & \text{otherwise}. \end{cases} \tag{5}$$

Following Pepper,[25] the volumetric absorptance $\eta(z)$ is given by the negative divergence of the Poynting vector $\mathbf{S}(z)$ of the electromagnetic field at the position z divided by the incident flux S_0,

$$\eta(z) = -\frac{\nabla \mathbf{S}(z)}{S_0}, \tag{6}$$

and can be derived within the Fresnel formalism to[11]

$$\eta(z) = \frac{2\xi'\xi''}{\xi_0}\{|T|^2 \exp(-2\xi''z)|R|^2 \exp(+2\xi''z) + 2\,\mathrm{Re}[(T^*R)\exp(-2i\xi'z)]\}, \tag{7}$$

where T and R are complex coefficients describing the transmission and reflection of the electromagnetic field in the media, respectively,[11] $\xi'=\mathrm{Re}\{\xi\}$, $\xi''=\mathrm{Im}\{\xi\}$, $\xi=(2\pi/\lambda_0)\sqrt{\epsilon}$, $\xi_0=2\pi/\lambda_0$, and $\epsilon=(n+ik)^2$. Here, λ_0 is the wavelength of the electromagnetic field, and n and k are the refractive and the absorption indices of the media, respectively. For the present system, the following numerical values have been assumed: $n=1.37$, $k=1.38$ for Ag,[28] $n=1.834$, $k=0$ for AlO_x,[29] and $n=0.21$, $k=3.11$ for Al.[30]

2. Charge transport in the metal

For the charge transport in the metal films, we consider only ballistic charge carriers, i.e., electrons (holes) which

reach the metal-insulator interface without being (inelastically) scattered. The reason behind this simplification is that most of the carriers suffering one or more inelastic scattering processes are expected to reach the interface with low energy, thus having a much lower probability to overcome the oxide barrier. One further assumption in our model is that the optically excited carriers propagate isotropically in all directions. Additionally, quasielastic (electron-phonon) scattering has been neglected.

The probability $P_{\text{tr}}(E,\theta,z)$ of an electron excited with energy E to reach the metal-insulator interface from a distance Δz under an angle θ without scattering is[31]

$$P_{\text{tr}}(E,\theta,z) = \frac{1}{2}\exp\left(-\frac{\Delta z}{\lambda_{ee}(E)\cos\theta}\right), \tag{8}$$

where $\lambda_{ee}(E)$ is the inelastic mean free path of the electrons in the metal, and the factor $\frac{1}{2}$ denotes that only half of the excited carriers are oriented toward the metal-insulator interface. In the neighborhood of the Fermi level, Quinn[32] derived within the random phase approximation (RPA) of the general Fermi liquid theory the following relation:

$$\lambda_{ee}(E) = \lambda_0^{\text{RPA}}(r_s)\frac{(E+E_F)E_F}{E^2}, \tag{9}$$

with $\lambda_0^{\text{RPA}}(r_s) \approx 4(1+r_s)$ in a.u.,[33] where $r_s=3.02$ a.u. for Ag and $r_s=2.07$ a.u. for Al.[27]

Knowing the number of photons incident per unit time, N_0, on the surface of area A_0, one can calculate the number of electrons $N_{\text{int}}(E,z)$ with energy E per unit time reaching the interface under an angle θ as

$$N_{\text{int}}(E,\theta) = N_0\int_0^{d_M} P_{\text{tr}}(E,\theta,z)P_{\text{exc}}(E,z)dz, \tag{10}$$

where d_M is the thickness of the metal film.

3. Charge transport through the oxide

For the transmission through the oxide layer, we assumed a probability $P_{\text{tun}}=1$ for electrons (holes) located in energy states above the respective barrier, while for tunneling through the barrier, the transmission probability was calculated in the WKB approximation:[34]

$$P_{\text{tun}}(E,\theta,U) = \exp\left[-2\int_0^{d_{\text{ox}}}[-k_z^2(E,\theta,z',U)]^{1/2}dz'\right], \tag{11}$$

where k_z is the electron wave number normal to the film plane and d_{ox} is the thickness of the oxide layer. In order to determine k_z, we employed the dispersion relation given by Gundlach[34] in the two-band model of Franz[15] and Kane and Blount:[16]

$$k_z^2 = \frac{2m}{\hbar^2}\frac{[E-V(U,z')][E-V(U,z')+E_g]}{E_g} - k_\parallel^2, \tag{12}$$

where m is the effective mass of the carrier in the insulator, which is assumed here to be equal to the mass of the free electron, E is the energy of the carrier, $V(U,z')$ denotes the bottom of the conduction band at a voltage U and position z', and E_g is the width of the band gap of the insulator. Between the wave number parallel to the film plane, $k_\parallel$, and the corresponding energy $E_\parallel$, the parabolic dependence

$$k_\parallel = \frac{2m}{\hbar^2}E_\parallel \tag{13}$$

is assumed. Additionally, from energy conservation,

$$E_\parallel = E + E_F - E_z, \tag{14}$$

where E_z is the energy associated with the carrier transport along the z direction. Integrating over θ and making the substitutions $\cos\theta=[E_z/(E+E_F)]^{1/2}$ and $k_\parallel^2=(2m/\hbar^2)(E+E_F-E_z)$, one obtains the number of electrons with energy E detected in the opposite electrode as follows:

$$N(E,U) = \begin{cases} \frac{1}{2}(E+E_F)^{-1/2}\int_{E_0(U)}^{E_F+E} E_z^{-1/2}N_{\text{int}}(E,E_z)P_{\text{tun}}(E,E_z,U)dE_z & \text{when} \quad E > \max(0,-eU) \\ 0 & \text{when} \quad E < \max(0,-eU), \end{cases} \tag{15}$$

where $E_0(U)=\max(0,E_{F_1}-E_{F_2}-eU)$ accounts for the step potential barrier induced by the difference in energy of the valence band bottom of the two metals. The case differentiation in Eq. (15) indicates that only electrons excited at energy states above the Fermi level of the opposite electrode are detected in the opposite electrode, since for electrons at energy states below this level, no available free states, allowing for tunneling, exist. It should be noted further that Eq. (15) does not include the dc bias current, Eq. (5) ensuring via Eqs. (10) and (15) that only electrons at energy states above the Fermi level are taken into account.

The electron current flowing from the top to the bottom electrode at an applied voltage U is then

$$I_e^{\text{Ag}\to\text{Al}}(U) = \int_0^{E_{\text{ph}}} eN(E,U)dE. \tag{16}$$

In the treatment of the holes, the following assumptions are made: (i) the zero point of the energy scale for holes is the same as for electrons, i.e., the Fermi level of the corresponding metal, (ii) the direction of the energy scale for holes is opposite to that for electrons, (iii) the mean free path of a hole with energy E below the Fermi level E_F is equal to the mean free path of an electron with energy E above the Fermi level, and (iv) the normalized distribution function $P_0(E)$ for holes with energy E below E_F is equal to that of electrons with energy $E_{\mathrm{ph}}-|E|$ above E_F. As a consequence, Eq. (5) changes in the case of holes to

$$P_0(E)=\begin{cases}\dfrac{3}{2E_F^{3/2}}(E_F-E)^{1/2} & \text{if}\quad 0<E<E_{\mathrm{ph}}\\ 0 & \text{otherwise}.\end{cases} \tag{17}$$

With the previously mentioned assumptions, no further changes have to be made to the model presented above in order to calculate the hole current flowing from the top to the bottom electrode, $I_h^{\mathrm{Ag}\to\mathrm{Al}}(U)$.

In an analogous way, the electron and hole currents $I_{e,h}^{\mathrm{Al}\to\mathrm{Ag}}(U)$ flowing from the bottom aluminum electrode to the top silver electrode can be calculated. It should be noted that, in this case, the lower integration limit of Eq. (15) is replaced by $\max(0,E_{F_2}-E_{F_1}+eU)$, while in the discriminating conditions, $-eU$ changes to eU.

The net current flowing through the oxide is then given by

$$I(U)=I_e^{\mathrm{Ag}\to\mathrm{Al}}(U)-I_h^{\mathrm{Ag}\to\mathrm{Al}}-I_e^{\mathrm{Al}\to\mathrm{Ag}}(U)+I_h^{\mathrm{Al}\to\mathrm{Ag}}(U), \tag{18}$$

where all currents in Eq. (18) have positive values.

The photo induced internal emission yield as defined in Sec. II is then given by

$$\gamma(U)=\frac{I(U)}{eN_0}=\gamma_{e,1}(U)+\gamma_{h,1}(U)+\gamma_{e,2}(U)+\gamma_{h,2}(U), \tag{19}$$

where N_0 is the incident photon flux, and $\gamma_{e,1}$, $\gamma_{h,1}$, $\gamma_{e,2}$, and $\gamma_{h,2}$ are the yields corresponding to $I_e^{\mathrm{Ag}\to\mathrm{Al}}$, $I_h^{\mathrm{Ag}\to\mathrm{Al}}$, $I_e^{\mathrm{Al}\to\mathrm{Ag}}$, and $I_h^{\mathrm{Al}\to\mathrm{Ag}}$, respectively.

4. Results

According to Eq. (19), there are four possible contributions to the net photo induced internal emission yield, corresponding to the two types of excited charge carriers (electrons and holes) and to the two directions of propagations (from Ag into Al and vice versa). Figure 7 shows the calculated bias dependence of the photo induced internal emission yield at $h\nu$=4.67 eV for the case when all four contributions are considered (scenario 1, squares). In addition, three other possible scenarios are illustrated: (i) when only the carriers excited in silver (scenario 2, circles), (ii) when only excited electrons from both metals (scenario 3, triangles), and (iii) when only excited electrons from silver (scenario 4, diamonds) are contributing to the induced current, respectively.

Scenario 1 represents the most realistic case in a photo excitation experiment. In order to simulate the experimental data, the following parameters of the oxide barrier (see inset of Fig. 8) were assumed in the calculations: Φ_{Al}=2.4 eV, Φ_{Ag}=3.9 eV,[20] and E_g=6.7 eV.[35] Here, the first two values have been determined from measurements on oxide layers prepared in the same way as in the present work,[20] while the numerical value for the band gap was taken from Ref. 35, being determined from optical measurements on an anodized aluminum oxide film. Despite the simplicity of the underlying model, the calculated data show a fairly good agreement with the experimental data (see Fig. 8), especially with respect to the absolute value of the emission yield. Remarkable is also the fact that the calculated curve shows a polarity change at about −0.6 V, which differs only by 0.1 V from the experimental value of −0.7 V. The simulated curve fails,

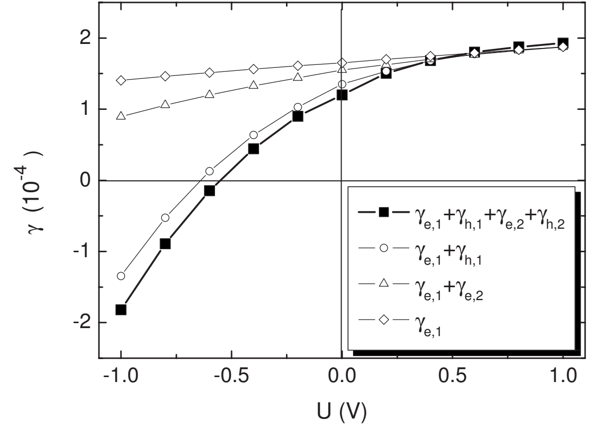

FIG. 7. Bias dependences of the internal photo emission yield in Ag-AlO_x-Al calculated under the following assumptions: (i) all contributions are considered (squares), (ii) only the contribution of the carriers excited in silver is considered (circles), (iii) the contribution of holes from both metals is neglected (triangles), and (iv) only the contribution of the excited electrons in silver is taken into account (diamonds). The partial contributions $\gamma_{1,e}$, $\gamma_{1,h}$, $\gamma_{2,e}$, and $\gamma_{2,h}$ are defined in Sec. IV A 3. Here, indices 1 and 2 denote the direction from Ag to Al and vice versa, respectively. The silver film thickness is taken to be 20 nm.

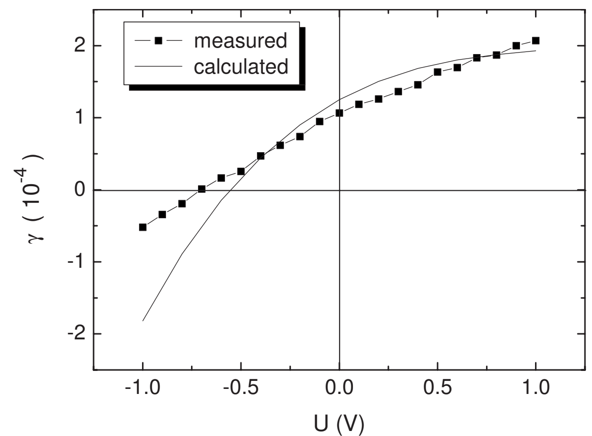

FIG. 8. Comparison between measured and calculated photo induced internal photo emission yield in a Ag-AlO_x-Al junction at a photon energy $h\nu$=4.67 eV. The thickness of the silver film was 20 nm.

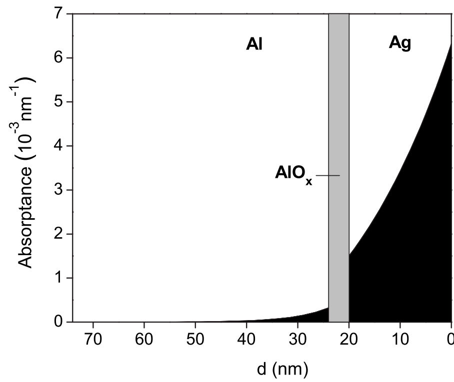

FIG. 9. Volumetric absorptance calculated for photons of energy $h\nu$=4.67 eV in a Ag-AlO_x-Al junction under normal incidence.

however, to explain the nearly linear shape of the experimental curve. As will be discussed in Sec. IV B, the potential barrier parameters may have a big influence on the shape of the $\gamma(U)$ curve. Thus, one reason for the mismatch between the calculated and the measured curve can be the uncertainty in the potential barrier parameters. At positive voltages, the calculated curve seems to reach a saturation value. This can be due to the fact that in the calculation, the barrier is rigid, meaning that the barrier heights Φ_{Al} and Φ_{Ag} do not change with applied bias voltage. In this case, the increased bias voltage has only a minor effect on the over-the-barrier transport and, hence, on the induced current. It is, however, well known[36] that the inclusion of an image potential would result in a lowering of the potential barrier heights by rounding off the corners and reducing the thickness of the barrier. With increasing bias voltage, the mean barrier height and the barrier thickness are further lowered.[36] The resulting enhancement of the over-the-barrier electron transport might then account for the experimentally observed behavior. Another reason may be an underestimation of the hole tunneling at higher positive voltages.

In scenario 2, the backward current is neglected. In this case, the calculated curve differs only slightly from the one calculated in scenario 1, with the yield changing sign at −0.7 V. This result indicates that the backward current has only a minor but not negligible influence on the yield. Moreover, it can be concluded that the holes excited in the top Ag film are responsible for the observed polarity change. Scenario 3, which neglects any hole transport across the oxide layer, supports this conclusion. It can be seen in Fig. 7 that a backward electron current only cannot explain the polarity change observed at −0.7 V. The possibility that the backward current is underestimated by the simulation, however, cannot be completely excluded. The last scenario, involving only electrons excited in the top Ag film, leads to a slight and practically linear thickness dependence of the yield in the investigated voltage range. At high negative voltages, the yield shows then an exponential decrease, excluding any possibility of sign change.

One reason for the weak backward current can be found in Fig. 9, which shows the volumetric absorptance calculated for the normal incidence of a laser light beam with a wavelength of 266 nm on a Ag-AlO_x-Al structure. The decrease with depth is exponential-like but does not simply follow the Beer-Lambert law of photo absorption, since in thin films back reflections and interference processes are not negligible. Since each photon is absorbed by one electron, the volumetric absorptance reflects also the spatial hot charge carrier distribution in the two metals. In Fig. 9, about 72% of the incident photons are absorbed in the silver film, while only about 2% are absorbed in the aluminum film. The rest is back reflected at the interfaces between the media into the vacuum. The volumetric absorption is seen to drop from the Ag-AlO_x interface to the Al-AlO_x interface by a factor of 4.5. This is partly due to the fact that the incoming light is strongly reflected at the Al-AlO_x interface. At the wavelength investigated here, the refractive index of aluminum is close to zero (n=0.21),[28] leading to a calculated reflectivity of about 63% at the Al-AlO_x interface. The relatively small amount of absorbed photons in the aluminum film indicates that less electron-hole pairs are excited in aluminum than in silver and implicitly a relatively low backward current is expected to flow through the oxide into the silver electrode.

One simplification introduced in the present model is the omission of the intrinsic field in the oxide, which is present in a MIM structure as a result of the different barrier heights at the two metal-oxide interfaces. In fact, Braunstein *et al.*[37,38] suggested that this built-in field may be responsible for the polarity change of the photo induced current in such a MIM structure. For photon energies larger than the barrier height, the mean free path of hot electrons is small compared to the thickness of the oxide as reported by Collins and Davies[39] and therefore electrons injected into the oxide will rapidly lose energy while traversing it. In the present case, this may lead to part (or most) of the electrons traveling against the field being repelled, thus effectively reducing $\gamma_{e,2}$ while $\gamma_{e,1}$ remains unchanged. In our system, the largest effect of the intrinsic field is to switch of the backward current $I_e^{Al\rightarrow Ag}$. In the absence of holes, this would correspond to the previously discussed scenario 4, which cannot explain the sign reversal. A similar observation was made by Gundlach and Kadlec,[12] who doubted the interpretation of Braunstein *et al.* and considered that the sign reversal is more likely to be due to hole emission, as previously also demonstrated by Goodman.[13] They concluded, however, that a detailed model should include the built-in field and an energy dependence of the mean free path in the oxide, as described by Crowell and Sze.[40] In our model, the presence of the intrinsic field would mean a strong reduction of the backward electron and the forward hole current, respectively. This situation corresponds again to scenario 4 and, hence, could not explain the observed sign change unless the intrinsic field would also change sign in the investigated voltage range.

In Fig. 10, the calculated and measured thickness dependences of the photo induced emission yield are compared. For a direct comparison, both data were normalized to the value of the yield at 20 nm. There is a good agreement between the experimental and the calculated data up to a thickness of about 45 nm. Above this value, the experimental data are a little bit higher than the calculated, and the difference between them is, however, of the same order as the experimental error. The decay constant of the exponential curves is about 14 nm, which is close to the value of about 16 nm

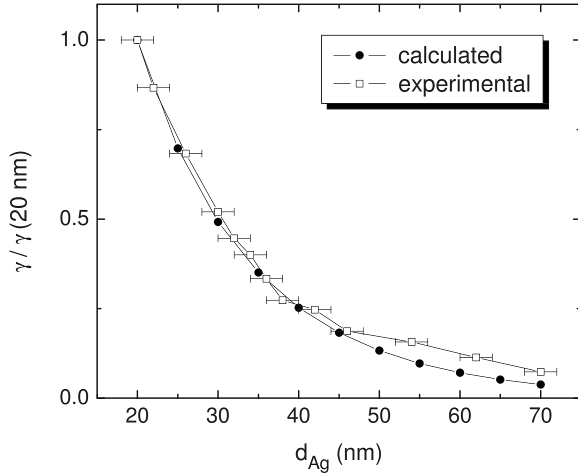

FIG. 10. Comparison between measured (squares) and calculated (circles) dependences of the photo induced internal emission yield on the silver film thickness in a Ag-AlO_x-Al junction. The photon energy was $h\nu=4.67$ eV.

predicted by the Beer-Lambert law, indicating that the induced tunneling current is practically determined by the attenuation of the incident light beam. In principle, this observation suggests that only electrons excited close to the silver-oxide interface substantially contribute to the measured yield. In particular, the contribution of hot charge carriers excited at distances exceeding 20 nm from the Ag-AlO_x interface is negligibly small. The analysis shows that the main contribution to the induced tunneling current is given by those carriers located in states above the potential barrier, i.e., with excitation energies of at least 3–4 eV. Since Eq. (9) predicts at these energies inelastic mean free paths of the carriers of only 3–4 nm, it is clear that only a very small part of the carriers excited at significantly larger distances will reach the Ag-AlO_x interface and overcome the barrier. Unfortunately, no experimental data are available for thicknesses of the silver film, which are comparable to the mean free path, since below 15 nm no closed films can be obtained at room temperature due to the nonepitaxial growth of silver on amorphous alumina.

B. Tunneling between two electron gases with different temperatures in two-band tunnel systems

While the photo conduction can be described within a three-step model (photo absorption, charge transport in the metal, and charge transport through the oxide), the particle induced conduction is a more complex process: a particle loses only a part of its energy to the electrons, whereas the other part is dissipated directly to elastic collisions or phonons. Additionally, the locus of electronic excitation is not well defined but smeared out along the trajectory of the incoming particle. A detailed description of the energy transfer from kinetic to electronic energy ("electronic stopping") is complicated and clearly beyond the scope of this paper. For the present discussion, we describe the particle induced electronic excitation as a Fermi distribution with temporally and locally elevated electron temperature within the top Ag electrode, whereas the bottom Al electrode remains at room temperature.

1. Two-temperature model

In a metal-insulator-metal sandwich structure, the net tunneling current density j through the insulator may be written as[41]

$$j=\frac{4\pi me}{h^3}\int_0^\infty [f_1(E)-f_2(E)]dE\int_0^E P_{\text{tun}}(E,E_\parallel)dE_\parallel, \quad (20)$$

where $E_\parallel$ is the energy component parallel to the film plane, $f_1(E)$ and $f_2(E)$ are the occupation probabilities for electron states in the two metal films, m is the electron mass, e is the elementary charge, and $P_{\text{tun}}(E,E_\parallel,U)$ is the transmission probability.

By applying a bias voltage U between the two metal electrodes and assuming that tunneling of the carriers takes place between two electron gases with temperatures T_1 and T_2, the occupation probabilities f_1 and f_2 have to be written as

$$f_1(E,U,T_1)=\left[\exp\left(\frac{E-eU}{k_BT_1}\right)+1\right]^{-1}, \quad (21)$$

$$f_2(E,T_2)=\left[\exp\left(\frac{E}{k_BT_2}\right)+1\right]^{-1}, \quad (22)$$

where k_B is the Boltzmann constant and E is defined with respect to the Fermi energy of the bottom electrode. Thus, Eq. (20) becomes

$$j(U,T_1,T_2)=\frac{4\pi me}{h^3}\int_{E_0(U)}^\infty [f_1(E,U,T_1)-f_2(E,T_2)] \times\left(\int_0^{E-E_0(U)} P_{\text{tun}}(E,E_\parallel,U)dE_\parallel\right)dE, \quad (23)$$

where $P_{\text{tun}}(E,E_\parallel,U)$ is the transmission probability through the barrier as defined in Eq. (11). Here, the lower integration limit in the first integral $E_0(U)=\max(-E_{F_2},eU-E_{F_1})$ ensures that no integration is performed over energies below the valence band of the two electrodes, where no electronic states exist in our model. The upper limit of the second integral relates to the condition that only electrons with the energy component perpendicular to the film plane higher than $E_0(U)$ can overcome the tunnel barrier.

2. Results

Figure 11 shows the bias dependence of the normalized current density in a Ag-AlO_x-Al junction calculated within the previously presented model. The Al electrode is represented by a free-electron gas at $T=300$ K, whereas the top electrode is represented as a free-electron gas at electron temperatures of 800, 4000, and 12 000 K. At 800 K, the tunneling current strongly increases with increasing positive voltage. At 4000 K, the current increases only slightly and almost linearly in the positive voltage region, while for negative voltages, it strongly decreases showing a polarity change at −0.35V. At 12 000 K, the normalized tunneling current

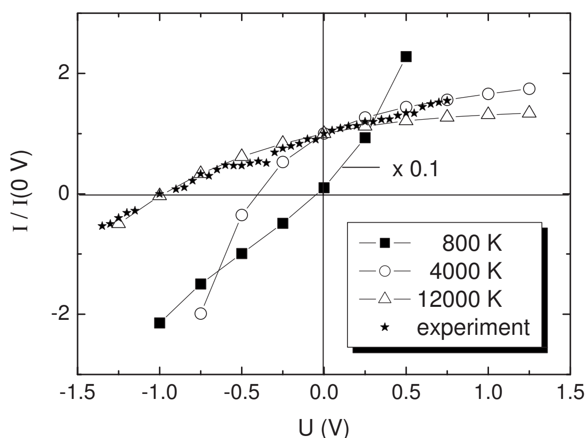

FIG. 11. Calculated bias dependence of the normalized tunneling current density $I/I(0\text{ V})$ flowing between two free-electron gases of temperatures T and 300 K, respectively, plotted for 800 K (squares), 4000 K (circles), and 12 000 K (triangles). For comparison, the measured normalized tunneling current (stars) induced by Ar^+ ions with a kinetic energy of 12 keV in a Ag-AlO_x-Al junction is also plotted.

density resembles the measured normalized tunneling current density quite well up to about 0.5eV. Above this voltage, the calculated curve seems to saturate at some maximum value, while the experimental curve further increases.

Within the two-temperature model, it can be shown that the sign change of the tunneling current (crossover point) always occurs at 0 V for a symmetric and rectangular tunneling barrier independent of the two electron gas temperatures. This changes when a higher barrier exists for holes than for electrons. Thus, at low temperatures, e.g., 800 K, most of the charge carriers are excited at energy levels lower than the corresponding barrier height. Since the barrier height for holes is higher than for electrons, the crossover point slightly shifts to a negative value. At this temperature, however, most of the carriers are excited far below the barrier edges and the transport is determined by tunneling processes. Thus, the transmission probability through the barrier is strongly influenced by the bias voltage as presented in Fig. 11. This influence is observed to become weaker with increasing temperature. At 4000 K, for instance, the induced current increases only slightly at positive bias voltages, while at negative values, the curve is strongly bent due to the increased importance of the hole tunneling. The crossover point is found here to be close to −0.5 eV. Since this value still does not resemble the experimental one, we further increased the temperature and found that the two mentioned values coincide if the temperature is set to 12 000 K. It can be seen in Fig. 11 that the calculated bias dependence fits, in this case, the experimental one remarkably well, indicating that a nearly linear dependence only occurs when the transport over the barrier becomes the dominant process. It appears, however, very improbable that an electron gas reaches such a high temperature during interaction with the argon ions, and, hence, care must be taken in interpreting this results. This becomes clear by observing that the calculated current density is of the order of 10^{12} A/m^2. A more reasonable agreement between experiment and simulation can be obtained by slightly varying the barrier parameters. It has been shown that, by setting the barrier height at the Ag-AlO_x interface to 3.3 eV instead of 3.9 eV, the experimental data in Fig. 11 could be fitted best for an electron temperature of about 4000 K.[24]

It can be argued that some Ar^+ ions with a kinetic energy of 12 keV may penetrate the bottom Al film. Indeed, transport of ions in matter (TRIM) calculations[42] predict that about 10^{-3} of the ions may reach the bottom electrode. The possibility that the observed polarity change is due to a reverse current of electrons flowing from Al into Ag can be ruled out, however, due to several reasons. First, similar results were found recently in experiments with argon ions of 1 keV (Ref. 43) under normal incidence. In this case, the ions definitely do not enter the bottom Al film. TRIM calculations show that the ions cannot penetrate more than 8 nm deep in the top Ag film. A second argument is the unavoidable damage of the oxide layer. Thus, an important amount of argon ions penetrating the oxide layer would lead to irreversible modifications in the structure of the oxide and, hence, to a measurable change in the current-voltage characteristics of the tunnel junction. This, however, was carefully avoided in the experiments presented here.

V. CONCLUSIONS

In conclusion, we have reported experimental results and model calculations on photon and heavy particle induced conduction in Ag-AlO_x-Al tunnel junctions at 4.7 eV and a kinetic energy of 12 keV, respectively. It was shown that both kinds of experiments lead to qualitatively similar results. The measured dependence of the induced current on the bias voltage applied across the tunnel junction can be explained by simultaneous contributions of electrons and holes excited in the silver film. The model calculations on photo induced conduction indicate that charge carriers excited in the aluminum film only play a minor role in the conduction process. Moreover, it is found that the linear shape of the bias dependence is characteristic for the transport of charge carriers (electrons and holes) above and below the respective tunnel barrier. The same seems to be true for kinetic excitation as well. In this case, the measured bias voltage dependence can be explained by assuming a locally and temporally heated electron gas in the bombarded metal film.

ACKNOWLEDGMENTS

The authors would like to thank Eckart Hasselbrink and Kristian Laß for the Nd:YAG laser and their support. The calculations were performed on JUMP (Jülich Multi Processor System) at Forschungszentrum Jülich. This work was supported by the DFG in the frame of the projects A3 and A4 of the SFB 616 “Energy Dissipation on Surfaces.”

*detlef.diesing@uni-duisburg-essen.de

[1] J. P. Spratt, R. F. Schwarz, and W. M. Kane, Phys. Rev. Lett. **6**, 341 (1961).
[2] H. Nienhaus, H. S. Bergh, B. Gergen, A. Majumdar, W. H. Weinberg, and E. W. McFarland, Phys. Rev. Lett. **82**, 446 (1999).
[3] B. Mildner, E. Hasselbrink, and D. Diesing, Chem. Phys. Lett. **432**, 133 (2006).
[4] S. Meyer, D. Diesing, and A. Wucher, Phys. Rev. Lett. **93**, 137601 (2004).
[5] D. Krix, R. Nünthel, and H. Nienhaus, Phys. Rev. B **75**, 073410 (2007).
[6] S. Meyer, D. Diesing, and A. Wucher, Nucl. Instrum. Methods Phys. Res. B **230**, 608 (2005).
[7] W. E. Spicer, Phys. Rev. **112**, 114 (1958).
[8] E. O. Kane, Phys. Rev. **127**, 131 (1962).
[9] E. O. Kane, Phys. Rev. **147**, 335 (1966).
[10] V. L. Dalal, J. Appl. Phys. **42**, 2274 (1971).
[11] J. Kadlec, Phys. Rep., Phys. Lett. **26**, 70 (1976).
[12] K. H. Gundlach and J. Kadlec, Thin Solid Films **28**, 107 (1975).
[13] A. M. Goodman, J. Appl. Phys. **41**, 2176 (1970).
[14] H. Momida, T. Hamada, Y. Takagi, T. Yamamoto, T. Uda, and T. Ohno, Phys. Rev. B **73**, 054108 (2006).
[15] W. Franz, *Handbuch der Physik* (Springer-Verlag, Berlin, 1956), Vol. 17, p. 155.
[16] E. O. Kane and E. I. Blount, *Tunneling Phenomena in Solids* (Plenum, New York, 1969), p. 79.
[17] K. W. Shepard, J. Appl. Phys. **36**, 796 (1965).
[18] Z. Burshtein and J. Levinson, Phys. Rev. B **12**, 3453 (1975).
[19] D. R. Jennison, P. A. Schultz, and J. P. Sullivan, Phys. Rev. B **69**, 041405(R) (2004).
[20] D. Diesing, G. Kritzler, M. Stermann, D. Nolting, and A. Otto, J. Solid State Electrochem. **7**, 389 (2003).
[21] H. D. Hagstrum, Phys. Rev. **96**, 325 (1954).
[22] M. Rösler and D. Hasselkamp, *Particle Induced Electron Emission*, Springer Tracts in Modern Physics Vol. 1 (Springer, Berlin, 1991).
[23] M. P. Seah and W. A. Dench, Surf. Interface Anal. **1**, 2 (1979).
[24] S. Meyer, A. Wucher, and D. Diesing (unpublished).
[25] S. V. Pepper, J. Opt. Soc. Am. **60**, 805 (1970).
[26] A. J. McAlister and E. A. Stern, Phys. Rev. **132**, 1599 (1963).
[27] N. Ashcroft and N. Mermin, *Solid State Physics* (Saunders, Philadelphia, 1976), Chap. 2, p. 38.
[28] P. B. Johnson and R. W. Christy, Phys. Rev. B **6**, 4370 (1972).
[29] H. Malitson, F. V. Murphy, and W. S. Rodeny, J. Opt. Soc. Am. **48**, 72 (1958).
[30] E. Shiles, T. Sasaki, M. Inokuti, and D. Y. Smith, Phys. Rev. B **22**, 1612 (1980).
[31] C. N. Berglund and W. E. Spicer, Phys. Rev. **136**, A1030 (1964).
[32] J. J. Quinn, Phys. Rev. **126**, 1453 (1962).
[33] K. Reuter, U. Hohenester, P. L. de Andres, F. J. García-Vidal, F. Flores, K. Heinz, and P. Kocevar, Phys. Rev. B **61**, 4522 (2000).
[34] K. H. Gundlach, J. Appl. Phys. **44**, 5005 (1973).
[35] E. T. Arakawa and M. W. Williams, J. Phys. Chem. Solids **29**, 735 (1968).
[36] J. G. Simmons, J. Appl. Phys. **34**, 1793 (1963).
[37] A. Braunstein, M. Braunstein, G. S. Picus, and C. A. Mead, Phys. Rev. Lett. **14**, 219 (1965).
[38] A. I. Braunstein, M. Braunstein, and G. S. Picus, Phys. Rev. Lett. **15**, 956 (1965).
[39] R. E. Collins and L. W. Davies, Solid-State Electron. **7**, 445 (1964).
[40] C. R. Crowell and M. Sze, Phys. Thin Films **4**, 325 (1967).
[41] R. Stratton, J. Phys. Chem. Solids **23**, 1177 (1962).
[42] Information on the SRIM2006 program package can be found at http://www.srim.org
[43] D. Kovacs, A. Golczewski, F. Aumayr, J. Winter, and D. Diesing (unpublished).